Deterministic single-phonon-to-photon quantum transducer for distributed quantum networks

Zhengyi Yue,[1] Tao Li,[1,2,*] Zhenhua Li,[1,2,†] and Keyu Xia[3,4,‡]

[1]*MIIT Key Laboratory of Semiconductor Microstructure and Quantum Sensing, School of Physics, Nanjing University of Science and Technology, Nanjing 210094, China*

[2]*Engineering Research Center of Semiconductor Device Optoelectronic Hybrid Integration in Jiangsu Province, Nanjing 210094, China*

[3]*College of Engineering and Applied Sciences, National Laboratory of Solid State Microstructures, Nanjing University, Nanjing 210023, China*

[4]*Shishan Laboratory, Suzhou Campus of Nanjing University, Suzhou 215000, China*

(Received 16 July 2024; revised 19 December 2024; accepted 10 February 2025; published 20 February 2025)

Quantum transducers are essential for connecting hybrid quantum systems with distinct frequencies, pivotal for hybrid quantum networks. A deterministic quantum transducer protocol is proposed for the upconversion of single phonons in the microwave domain to optical photons. Utilizing a hybrid optomechanical crystal coupled to a three-level emitter, the protocol deterministically upconverts an itinerant phonon into an optical photon, when an auxiliary optical cavity mode is driven by a single photon. Furthermore, the deterministic upconversion transducer can also be achieved by driving the emitter with a classical laser pulse, rather than driving the optical cavity with a single photon. The intracavity photon numbers in both protocols are significantly less than one during the operation, thus overcoming the problem of parasitic heating within radiation-pressure coupling of hybrid optomechanical systems. These outstanding features make the protocols particularly useful for the realization of large-scale distributed hybrid quantum networks.

DOI: 10.1103/PhysRevA.111.022623

I. INTRODUCTION

Hybrid quantum systems integrate the distinguished features of different physical subsystems [1–10], leveraging their strengths for practical quantum technologies while mitigating their inherent limitations. Superconducting circuits, operated in the microwave domain, are a promising system for quantum computing [11,12]. These circuits have achieved high-fidelity single- and two-qubit gates, and even error-corrected logical gates [13–17]. However, connecting two remote superconducting circuits remains a formidable challenge due to significant loss and noise during microwave photon transmission [18–21]. Quantum transduction, the process of interconverting quantum states across different physical systems [22–24], plays a vital role in bridging this gap, especially in hybrid quantum systems with significant eigenfrequency differences. The efficient and coherent conversion of microwave photons to optical photons [25–28] is a critical interface for distributed hybrid quantum networks [29–32], facilitating the exchange of quantum states between remotely separated superconducting quantum processors through low-loss optical fiber channels in room-temperature environments.

Optomechanical resonators utilize engineered mechanical systems strongly coupled to optical or microwave fields [33–45] and have shown promise in a variety of quantum applications. Single phonons at gigahertz (GHz) with a speed about five orders of magnitude slower than the speed of photons exhibit wavelengths comparable to optical photons, and thus feature distinct advantages over photons for on-chip quantum communications [46–51]. They serve as a promising alternative to microwave photons for implementing a coherent quantum bus connecting local artificial qubits within a single quantum chip [46–51], and have been extensively researched, such as nonclassical phononic states generation [52–58], unconventional spin-phonon interactions [59–66], and efficient microwave-to-optical transduction [67].

Phonon-to-photon quantum transducers in combination with photon-to-phonon quantum transducers enable optical connection of two spatially separated quantum chips for scalable quantum networking and distributed quantum computing [46–51]. Typically, these transducer schemes depended on the radiation pressure and mechanical backaction [33], with the strength proportional to the square root of the photon numbers in the cavity mode pumped by continuous-wave laser probes. However, for phononic modes in the microwave domain, the high number of intracavity photons can lead to significant optical absorption heating at sub-Kelvin temperatures [68–71]. Additionally, narrowband filters were necessary to remove unscattered pump modes [67–70] for the heralded generation and measurement of a single phonon upon the detection of an upconverted or a downconverted photon.

A single photon-to-phonon quantum transducer protocol [72] without radiation-pressure coupling was presented by engineering a hybrid optomechanical crystal and simultaneously coupling it to a three-level emitter across both photonic and phononic cavity modes [73]. An itinerant phonon can be deterministically generated by directly scattering a single optical

*Contact author: tao.li@njust.edu.cn
†Contact author: lizhenhua@njust.edu.cn
‡Contact author: keyu.xia@nju.edu.cn

photon without involving continuous-wave pumping in cavity modes, which eliminated parasitic heating in photon-to-phonon quantum transducers. However, the phonon-to-photon quantum transducer without radiation-pressure coupling remains yet to be demonstrated.

In this article, we introduce two deterministic protocols for implementing single phonon-to-photon quantum transducers without radiation-pressure coupling. Utilizing a hybrid optomechanical resonator that supports both photonic and phononic cavity modes, coupled to a three-level emitter [62,72], we achieve deterministic upconversion of an itinerant phonon into an optical photon, which is resonant with one optical transition frequency of the emitter when the cavity mode, resonant with the other optical transition, is probed by a single photon. Furthermore, we show that the single phonon-to-photon upconversion can also be achieved by driving the emitter with a classical laser pulse, instead of driving the cavity mode with a single photon [33]. In both protocols, the average intracavity photon number remains well below 1, and the influence of the optical absorption-induced phonon bath occupation is negligible [67–70]. Our deterministic single phonon-to-photon upconversion protocols, in combination with efficient photon-to-phonon downconversion protocols [72], paves the way for the development of large-scale distributed hybrid quantum networks [47–51].

II. DETERMINISTIC SINGLE PHONON-TO-PHOTON QUANTUM TRANSDUCER

The implementation of our deterministic single phonon-to-photon transducer is based on a hybrid optomechanical resonator with its phononic and optical modes, with resonance frequencies ω_a and ω_c, coupling to two transitions of a three-level emitter, respectively, shown in Fig. 1. The emitter can be a single charged quantum dot embedded in an optomechanical crystal in a magnetic field directed perpendicularly to its axis [72]. The transition between two ground states ($|1\rangle$ and $|2\rangle$) of the emitter couples to the phononic cavity mode $\hat{a}$ with coupling rate g_{21} and transition frequency ω_{21}. The optical transition of $|1\rangle$ to the excited state $|3\rangle$ with frequency ω_{31} couples to the optical cavity mode $\hat{c}$ with coupling rate g_{31}. The semi-infinite phononic and photonic waveguides exclusively couple to their respective modes of the optomechanical resonator with coupling rate κ_{21} and κ_{31} [74]. In the overcoupled regime for both the phononic and optical modes, the dominant resonator losses are channeled into phononic and photonic waveguides. The intrinsic resonator losses into nonguided modes can be neglected for simplicity [68,72]. Meanwhile, the emitter-resonator coupling is in the bad cavity but high cooperativity regime, with $\kappa_{ij} \gg g_{ij}, \gamma_i$ and $2g_{ij}^2/\kappa_{ij}\gamma_i \gg 1$ for $i = 2, 3$ and $j = 1, 2$ [72].

A. Type-I quantum transducer: Converting single phonons to photons by pumping a cavity mode with a single photon

In this section, we show that the deterministic single phonon-to-photon transducer can be achieved by pumping an auxiliary cavity mode, nearly resonant with the emitter, by a single photon. The auxiliary optical cavity mode $\hat{b}$ with resonance frequency ω_b couples to the emitter transition $|2\rangle \leftrightarrow |3\rangle$ and the photonic waveguide with coupling rates g_{32} and κ_{32},

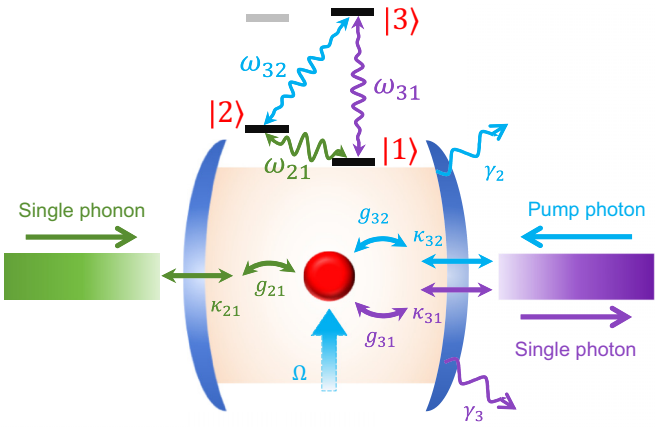

FIG. 1. Schematic of the single phonon-to-photon quantum transducer. The transitions ($|1\rangle \leftrightarrow |2\rangle$ and $|1\rangle \leftrightarrow |3\rangle$) of three-level emitter couple to the phononic and photonic modes ($\hat{a}$ and $\hat{c}$) of the optomechanical resonator with coupling strengths (g_{21} and g_{31}). The coupling strengths (κ_{21} and κ_{31}) denote the directional decay into the phononic and photonic waveguides. γ_2 (γ_3) is the spontaneous decay rate of the emitter state $|2\rangle$ ($|3\rangle$). (i) For the phonon-to-photon quantum transducer with single-photon driving, the auxiliary cavity mode $\hat{b}$ is involved and couples to the photonic waveguide with the input coupling rate κ_{32}, and couples to the emitter transition $|2\rangle \leftrightarrow |3\rangle$ with coupling strength g_{32}. (ii) For the phonon-to-photon quantum transducer with a classical pump, a laser pulse nearly in resonance drives the transition $|2\rangle \leftrightarrow |3\rangle$ of the emitter with the Rabi frequency Ω, and no auxiliary cavity mode $\hat{b}$ is involved.

respectively. The effective Hamiltonian $\hat{H}_{\rm eff}$ of the system, consisting of one emitter, one phononic, and two photonic cavity modes, can be expressed in the rotating frame as

$$\begin{aligned}\hat{H}_{\rm eff} =& \hbar\left(\delta_{21} - i\frac{\gamma_2}{2}\right)|2\rangle\langle 2| + \hbar\left(\delta_{31} - i\frac{\gamma_3}{2}\right)|3\rangle\langle 3| \\ &+ \hbar(\Delta_a - i\kappa_{21})\hat{a}^\dagger\hat{a} + \hbar(\Delta_b - i\kappa_{32})\hat{b}^\dagger\hat{b} \\ &+ \hbar(\Delta_c - i\kappa_{31})\hat{c}^\dagger\hat{c} - [i(\hbar g_{21}|2\rangle\langle 1|\hat{a} \\ &+ \hbar g_{32}|3\rangle\langle 2|\hat{b} + \hbar g_{31}|3\rangle\langle 1|\hat{c}) + \text{H.c.}], \end{aligned} \tag{1}$$

where $\delta_{21} = \omega_{21} - \omega_a$ ($\delta_{31} = \omega_{31} - \omega_c$) is the detuning between the emitter transition and the cavity mode; $\Delta_j = \omega_j' - \omega_j$ for $j = a, b, c$ is the detuning of the input and output mode with frequency ω_j' from the respective cavity mode; and γ_2 (γ_3) is the spontaneous decay rate of the emitter state $|2\rangle$ ($|3\rangle$) into other modes out of the optomechanical resonator.

In practice, the dissipative time evolution of the emitter and optomechanical resonator can be separated into an evolution with such an effective non-Hermitian Hamiltonian $\hat{H}_{\rm eff}$ interrupted by random quantum jumps [75–77]. These quantum jumps correspond in our model to nondirectional loss of either the photon or phonon out of the composite system by spontaneous decay of the emitter [78–80]. For calculating the transmission coefficients [80–83], we focus on the conditional dynamics described by the non-Hermitian Hamiltonian $\hat{H}_{\rm eff}$ without quantum jumps since the dissipation results in detectable photon or phonon loss and thus simultaneous vanishing transmission coefficients for the input phonon and desired output photon [78–83]. Note that these

nonzero decay rates present in the transmission coefficients and lead to a decrease in the sum of the square moduli of the transmission coefficients, indicating the influence of dissipation on the conditional dynamics.

We focus on analytically calculating the transmission coefficients by considering the dissipative evolution of the composite system using the Schrödinger equations. These transmission coefficients can also be calculated using the Heisenberg picture without dissipation [84]. In that case, the detunings are replaced with effective detunings that incorporate spontaneous decays as imaginary values in the resulting coefficients [80,85].

Suppose the emitter coupled to the optomechanical resonator in the frequency resolved limit (i.e., $\kappa_{21}, \kappa_{31}, \kappa_{32} \ll \omega_{21}$), where the coupling between nonresonant frequencies is assumed to be negligible [33,86]. When an itinerant phonon is directed to the phononic cavity mode by the phonon waveguide and a single photon pumps the cavity mode $\hat{b}$, the composite system, with the emitter initialized in the state $|1\rangle$, evolves under the effective non-Hermitian Hamiltonian $\hat{H}_{\rm eff}$. Its general state can be expanded within *the subspace of interest*, instead of a complete subspace, without quantum jumps as

$$|\Psi\rangle = C_{21}\hat{a}^\dagger\hat{b}^\dagger|\emptyset,1\rangle + C_{32}\hat{b}^\dagger|\emptyset,2\rangle + C_{31}\hat{c}^\dagger|\emptyset,1\rangle + C_3|\emptyset,3\rangle. \tag{2}$$

Here $|\emptyset\rangle$ is the vacuum state of the phononic and photonic cavity modes. C_{21}, C_{32}, and C_{31} are the excited amplitudes of the cavity modes $\hat{a}\hat{b}$, $\hat{b}$, and $\hat{c}$, respectively. C_3 denotes the amplitude of the emitter in the excited state $|3\rangle$ and the cavity modes in the vacuum state $|\emptyset\rangle$.

The dynamics of the composite system is determined by the Schrödinger equation and the standard input-output relations [81–83]. We have the specified equations of motion for the amplitudes

$$\begin{aligned}
\dot{C}_{21} &= g_{21}C_{32} - i(\Delta_a - i\kappa_{21})C_{21} - i(\Delta_b - i\kappa_{32})C_{21} \\
&\quad + \sqrt{2\kappa_{21}}\beta_{ka}^{\rm in} + \sqrt{2\kappa_{32}}\beta_{kb}^{\rm in}, \\
\dot{C}_{32} &= -g_{21}C_{21} - i\left(\delta_{21} - i\frac{\gamma_2}{2}\right)C_{32} - i(\Delta_b - i\kappa_{32})C_{32} \\
&\quad + g_{32}C_3 + \sqrt{2\kappa_{32}}\beta_{kb}^{\rm in}, \\
\dot{C}_{31} &= -i(\Delta_c - i\kappa_{31})C_{31} + g_{31}C_3, \\
\dot{C}_3 &= -i\left(\delta_{31} - i\frac{\gamma_3}{2}\right)C_3 - g_{31}C_{31} - g_{32}C_{32},
\end{aligned} \tag{3}$$

where $\beta_{ka}^{\rm in}$ ($\beta_{kb}^{\rm in}$) is the probability amplitude of the input single phonon (photon) with a suitably long duration and frequency ω_a' (ω_b') that is nearly resonant to the cavity resonance mode $\hat{a}$ ($\hat{b}$) [81], and is related to the output amplitude $\beta_{ka}^{\rm out}$ ($\beta_{kb}^{\rm out}$, $\beta_{ka}^{\rm out'}$) as follows:

$$\begin{aligned}
\beta_{ka}^{\rm out} &= \sqrt{2\kappa_{21}}C_{21} - \beta_{ka}^{\rm in} = t_{21}\beta_{ka}^{\rm in}, \\
\beta_{kb}^{\rm out} &= \sqrt{2\kappa_{32}}C_{32} - \beta_{kb}^{\rm in} = t_{32}\beta_{kb}^{\rm in}, \\
\beta_{ka}^{\rm out'} &= \sqrt{2\kappa_{31}}C_{31} = t_{31}\beta_{ka}^{\rm in}.
\end{aligned} \tag{4}$$

The transmission coefficient t_{21} (t_{32}) refers to elastic scattering for the input phonon (photon), while t_{31} refers to inelastic scattering and its modulus square represents the upconversion efficiency of the single phonon-to-photon quantum transducer.

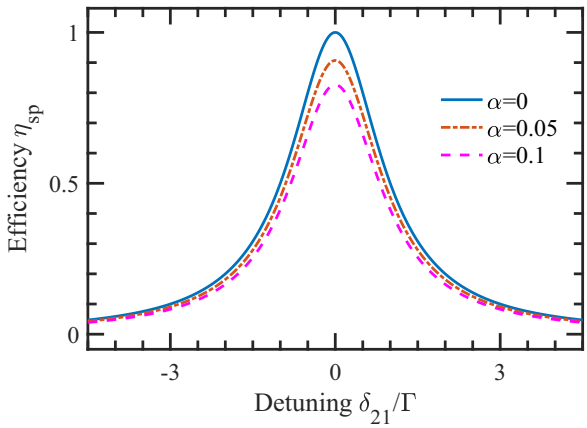

FIG. 2. Upconversion efficiency η_{sp} versus normalized detunings δ_{21}/Γ for the type-I quantum transducer. The solid, dashed, and dashed-doted curves are simulated for $\Gamma_{31}/\Gamma_{32} \simeq 1$ and $\alpha = 0, 0.05$, and 0.1, respectively.

These transmission coefficients can be found by considering the steady-state solution of the equations of motion, and thus we have

$$t_{21} = \frac{2[\varepsilon g_{21}\sqrt{\kappa_{21}\kappa_{32}} + (\varepsilon\sqrt{\kappa_{21}\kappa_{32}} + \kappa_{21})S_d]}{i\Delta_t S_d + g_{21}^2} - 1, \tag{5}$$

$$t_{32} = \frac{2[i\varepsilon\kappa_{32}\Delta_t - g_{21}(\sqrt{\kappa_{21}\kappa_{32}} + \varepsilon\kappa_{32})]}{\varepsilon\left(i\Delta_t S_d + g_{21}^2\right)} - 1, \tag{6}$$

$$t_{31} = \frac{2g_{31}g_{32}\sqrt{\kappa_{31}}[g_{21}(\sqrt{\kappa_{21}} + \varepsilon\sqrt{\kappa_{32}}) - i\varepsilon\sqrt{\kappa_{32}}\Delta_t]}{G\left(i\Delta_t S_d + g_{21}^2\right)}, \tag{7}$$

where $\tilde{\delta}_{21} = \delta_{21} - i\gamma_2/2$, $\tilde{\delta}_{31} = \delta_{31} - i\gamma_3/2$, $\tilde{\Delta}_a = \Delta_a - i\kappa_{21}$, $\tilde{\Delta}_b = \Delta_b - i\kappa_{32}$, $\tilde{\Delta}_c = \Delta_c - i\kappa_{31}$, $\Delta_t = \tilde{\Delta}_a + \tilde{\Delta}_b$, $G = g_{31}^2 - \tilde{\delta}_{31}\tilde{\Delta}_c$, $S_d = ig_{32}^2\tilde{\Delta}_c/G + i(\tilde{\Delta}_b + \tilde{\delta}_{21})$, and $\varepsilon = \beta_{kb}^{\rm in}/\beta_{ka}^{\rm in}$.

To achieve an efficient upconversion quantum transducer, the input single phonon and single photon are combined into the desired single photon with the sum frequency of the input phonon and photon. We assume that the input phonon and photon satisfy a mode matching condition $\varepsilon = -1$, under which the transmission coefficients $t_{21} = t_{32} = 0$ and $t_{31} = 1$ can be simultaneously achieved for vanishing detunings and decays (i.e., $\delta_{21} = \delta_{31} = \Delta_{\rm a} = \Delta_{\rm b} = \Delta_{\rm c} = 0$ and $\gamma_2 = \gamma_3 = 0$). When all detunings vanish and the conditions $t_{21} = t_{32} = 0$ are satisfied, the efficiency of the type-I quantum transducer, $\eta_{si} = |t_{31}|^2$, is simplified to

$$\eta_{si} = \frac{\Gamma_{31}\Gamma_{32}}{(\gamma_3 + \Gamma_{31})^2}, \tag{8}$$

where $\Gamma_{32} = 2g_{32}^2/\kappa_{32}$ and $\Gamma_{31} = 2g_{31}^2/\kappa_{31}$ represent the cavity-enhanced effective decay rates of the excited state $|3\rangle$ into the cavity modes $\hat{b}$ and $\hat{c}$, respectively. Note that a boundary condition $\Gamma_{32} < (\Gamma_{31} + \gamma_3)$ is implicitly required to satisfy the conditions $t_{21} = t_{32} = 0$, as detailed in Appendix A. For a large coupling efficiency with $\gamma_3 \ll \Gamma_{31}$ and balanced cavity-enhanced decay rates $\Gamma_{31} \simeq \Gamma_{32}$, a deterministic single phonon-to-photon quantum transducer can be achieved with near-unity efficiency, as shown in Fig. 2.

B. Type-II quantum transducer: Converting single phonons to photons by driving the emitter with a classical laser pulse

An alternative approach to achieve a deterministic single phonon-to-photon transducer can be implemented by driving the emitter with a classical laser pulse, instead of pumping the auxiliary cavity mode $\hat{b}$ with a single photon. We assume that the optomechanical resonator has one phononic mode $\hat{a}$ and one photonic mode $\hat{c}$, as shown in Fig. 1. The optomechanical resonator does not need to support the auxiliary mode b, and all parameters associated with mode $\hat{b}$ are vanishing (i.e., $\kappa_{32} = g_{32} = 0$). A laser pulse at the resonance frequency ω_{32} drives the transition $|2\rangle \leftrightarrow |3\rangle$ of the emitter with a Rabi frequency Ω.

The effective Hamiltonian of the system consisting of the phononic mode $\hat{a}$, the photonic mode $\hat{c}$, and the emitter can be described as [81–83]

$$\hat{H}'_{\rm eff} = \tilde{\delta}_{21}|2\rangle\langle 2| + \tilde{\delta}_{31}|3\rangle\langle 3| + \tilde{\Delta}_a\hat{a}^\dagger\hat{a} + \tilde{\Delta}_c\hat{c}^\dagger\hat{c} - \left[\left(\frac{\Omega}{2}|3\rangle\langle 2| + ig_{31}|3\rangle\langle 1|\hat{c} + ig_{21}|2\rangle\langle 1|\hat{a}\right) + \text{H.c.}\right], \tag{9}$$

where all parameters are the same as that defined for the type-I quantum transducer. A general state of the system, with the emitter initialized in the state $|1\rangle$ and an input phonon resonant with the transition $|1\rangle \leftrightarrow |2\rangle$, can thus be expanded within a subspace without quantum jumps as

$$|\Psi\rangle = C_{21}\hat{a}^\dagger|\emptyset, 1\rangle + C_{31}\hat{c}^\dagger|\emptyset, 1\rangle + C_2|\emptyset, 2\rangle + C_3|\emptyset, 3\rangle, \tag{10}$$

where C_2 (C_3) is the amplitude of the emitter in state $|2\rangle$ ($|3\rangle$) with zero phonon and photon, while C_{21} (C_{31}) denotes the amplitude of the emitter in state $|1\rangle$ with one phonon (photon).

The equations of motion for these amplitudes can be specified by the Schrödinger equation and the standard input-output relations as

$$\begin{aligned}
\dot{C}_{21} &= g_{21}C_2 - i(\Delta_a - i\kappa_{21})C_{21} + \sqrt{2\kappa_{21}}\beta_k^{\rm in},\\
\dot{C}_{31} &= g_{31}C_3 - i(\Delta_c - i\kappa_{31})C_{31},\\
\dot{C}_2 &= -i\left(\delta_{21} - i\frac{\gamma_2}{2}\right)C_2 + i\frac{\Omega}{2}C_3 - g_{21}C_{21},\\
\dot{C}_3 &= -i\left(\delta_{31} - i\frac{\gamma_3}{2}\right)C_3 + i\frac{\Omega}{2}C_2 - g_{31}C_{31}.
\end{aligned} \tag{11}$$

The output phononic (photonic) amplitude $\beta_k^{\rm out}$ ($\beta_k^{\rm out'}$) is related to the input phononic amplitude $\beta_k^{\rm in}$, and we have

$$\begin{aligned}
\beta_k^{\rm out} &= \sqrt{2\kappa_{21}}C_{21} - \beta_k^{\rm in} = t'_{21}\beta_k^{\rm in},\\
\beta_k^{\rm out'} &= \sqrt{2\kappa_{31}}C_{31} = t'_{31}\beta_k^{\rm in},
\end{aligned} \tag{12}$$

where t'_{21} and t'_{31} refer to the phononic and photonic amplitudes of the single-phonon scattering process. Therefore, $\eta_c = |t'_{31}|^2$ denotes the upconversion efficiency of the single phonon-to-photon quantum transducer.

These amplitudes for the steady-state solution of the equations of motion with the emitter driven by a classical laser field are

$$t'_{21} = \frac{2i\kappa_{21}(\Omega^2\tilde{\Delta}_c + 4\tilde{\delta}_{21}G)}{4g_{21}^2G - \tilde{\Delta}_a(\Omega^2\tilde{\Delta}_c + 4\tilde{\delta}_{21}G)} - 1, \tag{13}$$

$$t'_{31} = -\frac{4i\Omega g_{21}g_{31}\sqrt{\kappa_{21}\kappa_{31}}}{4g_{21}^2G - \tilde{\Delta}_a(\Omega^2\tilde{\Delta}_c + 4\tilde{\delta}_{21}G)}. \tag{14}$$

When all detunings are zero and the Rabi frequency of the driving field is $\Omega = \sqrt{(\Gamma_{21} - \gamma_2)(\Gamma_{31} + \gamma_3)}$, we have $|t'_{21}|^2 = 0$ and

$$\eta_{ci} = |t'_{31}|^2 = \frac{1 - \gamma_2/\Gamma_{21}}{1 + \gamma_3/\Gamma_{31}}, \tag{15}$$

which leads to a unity efficiency $\eta_c \simeq 1$ for vanishing detunings $\delta_{21} = \delta_{31} = \Delta_{\rm a} = \Delta_{\rm b} = \Delta_{\rm c} = 0$ and negligible spontaneous decay rates $\gamma_2/\Gamma_{21} \simeq 0$ and $\gamma_3/\Gamma_{31} \simeq 0$ [72].

III. PERFORMANCE ANALYSIS

So far, we show that the single phonon-to-photon quantum transducer driven by either a single photon or a classical laser pulse can be implemented with unity efficiency when all transitions are resonant and the spontaneous decay rates are negligible, compared to the cavity-enhanced decay rates. In this section, we show that our single phonon-to-photon transducer protocols can be efficiently implemented for practical parameters.

A. Performance of the type-I quantum transducer

We consider here the influence of the detuning, i.e., δ_{21} and the spontaneous decay on the performance. The practical efficiency of the single phonon-to-photon transducer $\eta_s = |t_{31}|^2$ can be specified as

$$\eta_{sp} = \frac{\Gamma^2}{(1+\alpha)^2\left(\Gamma^2 + \delta_{21}^2\right)}, \tag{16}$$

where the auxiliary parameters are $\Gamma = \kappa_{32}(2+\alpha)/(1+\alpha) + \gamma_2/2 + g_{21}^2/(\kappa_{21} + \kappa_{32})$, $\alpha = \gamma_3/\Gamma_{31}$.

The practical efficiencies η_{sp} versus normalized detunings δ_{21}/Γ for $\alpha = 0$, 0.05, 0.1 and $\Gamma_{31}/\Gamma_{32} \simeq 1$ are shown in Fig. 2. The maximal upconversion efficiency $\eta_{sp}^{\rm max}$ of the type-I phonon-to-photon transducer is achieved at the detuning zero with $\delta_{21}/\Gamma = 0$, and it decreases for increasing α. In particular, we have $\eta_{sp}^{\rm max} \simeq 1 - 2\alpha$ for $\alpha \ll 1$. For a mediate loss $\alpha = 0.05$, the upconversion efficiency $\eta_{sp} > 0.90$ can be achieved within a wide bandwidth of $\delta_{21}/\Gamma \in (-0.09, 0.09)$. For a constant Γ, the increase of α results in a smaller allowable amount of detuning to achieve a threshold upconversion efficiency, i.e., $\eta_{sp} \geqslant 0.5$ for implementing high-efficiency hybrid quantum networks.

B. Performance of the type-II quantum transducer

For the type-II quantum transducer driven by a classical laser pulse, we consider the influence of the detunings, δ_{21} and δ_{31}, on the upconversion efficiency, assuming $\delta_{21} = \delta_{31} = \Delta$. The upconversion efficiency $\eta_c = |t'_{31}|^2$ of the type-II transducer protocol can be specified as

$$\eta_{cp} = \left|\frac{\sqrt{(1-\beta)\alpha'}\Gamma_{21}\Gamma_{31}}{\alpha'\Gamma_{21}\Gamma_{31} - 2\Delta^2 + i\Delta[(1+\beta)\Gamma_{21} + \alpha'\Gamma_{31}]}\right|^2, \tag{17}$$

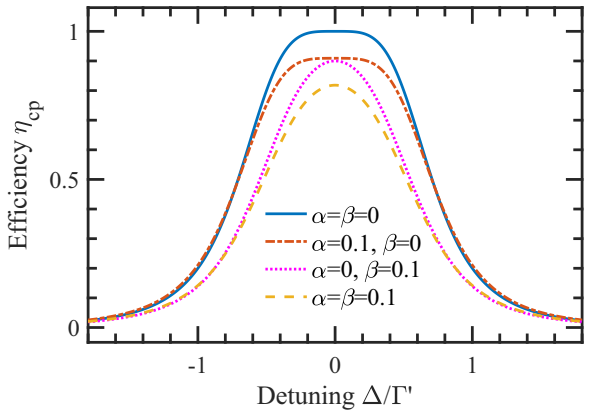

FIG. 3. Upconversion efficiency η_{cp} versus normalized detunings Δ/Γ' for the type-II quantum transducer with $\eta = 1$.

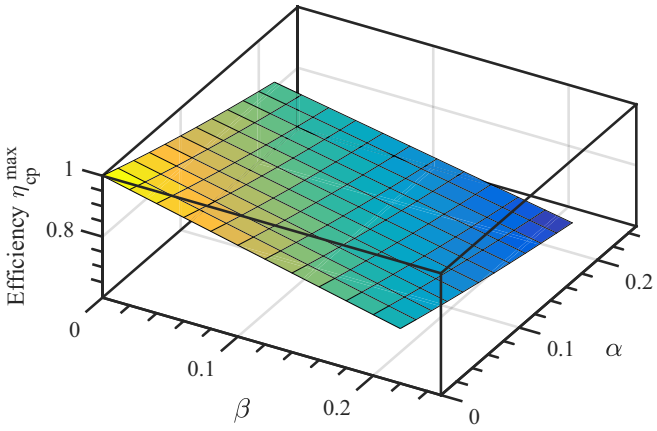

FIG. 4. Maximal upconversion efficiency $\eta_{cp}^{\max}$ versus normalized spontaneous decay rates α and β for the type-II quantum transducer. All detunings are assumed to be zero and $\eta = 1$ is used here.

where the auxiliary parameters are $\alpha' = 1 + \gamma_3/\Gamma_{31}$, $\beta = \gamma_2/\Gamma_{21}$, and $\Gamma' = (\Gamma_{21} + \Gamma_{31})/2$. Therefore, the maximal upconversion efficiencies $\eta_{cp}^{\max}$ can be specified as

$$\eta_{cp}^{\max} = \frac{1-\beta}{1+\alpha}, \tag{18}$$

which are achieved at vanishing detunings ($\Delta = 0$).

The upconversion efficiencies η_{cp} as functions of the normalized detuning Δ/Γ' for various normalized spontaneous decays α and β are shown in Fig. 3. The deterministic upconversion from a single phonon to the target photon can be achieved for vanishing detunings with $\Delta/\Gamma' = 0$, $\eta = \Gamma_{31}/\Gamma_{21} = 1$, and negligible spontaneous decays. Meanwhile, the upconversion efficiency $\eta_{cp} > 0.90$ can be achieved for a wide bandwidth of $\Delta/\Gamma' \in (-0.08, 0.08)$ for $\alpha = 0$ and $\beta = 0.1$. Furthermore, $\eta_{cp} \simeq \Gamma_{31}^4/(4\Delta^4 + \Gamma_{31}^4)$ for $\eta \simeq 1$ and the half-maximum width with $\eta_{cp} > 0.5$ is $\sqrt{2}\Gamma_{31}$. For the case of $\eta \ll 1$, $\eta_{cp} \simeq \eta^2\Gamma_{21}^4/(4\Delta^4 + \Delta^2\Gamma_{21}^2 + \eta^2\Gamma_{21}^4)$, where the half-maximum width becomes $2\Gamma_{31}$. In contrast, the half-maximum width is $2\Gamma_{21}$ for $\eta \gg 1$.

The influence of spontaneous decays relative to cavity-enhanced decays, α and β, on the maximal upconversion efficiency $\eta_{cp}^{\max}$ is shown in Fig. 4. In general, $\eta_{cp}^{\max}$ decreases as either α or β increases. However, the decrease in $\eta_{cp}^{\max}$ is less pronounced with increasing α compared to increasing β, indicating that phonon loss has a larger influence on the maximal conversion efficiency than photon loss. For example, when $\alpha = 0.1$ and $\beta = 0$, the maximal upconversion efficiency is approximately $\eta_{cp}^{\max} \simeq 0.91$, whereas for $\alpha = 0$ and $\beta = 0.1$, it is $\eta_{cp}^{\max} = 0.90$. Furthermore, for negligible spontaneous decays where $\alpha \ll 1$ and $\beta \ll 1$, the maximal upconversion efficiency can be approximated as $\eta_{cp}^{\max} \simeq 1 - \alpha - \beta$, which is a linear function of α and β and the influence of photon loss and phonon loss on $\eta_{cp}^{\max}$ becomes equal.

IV. DISCUSSION AND SUMMARY

We propose two deterministic protocols for the upconversion of single phonons into single photons employing two different pumping strategies within optomechanical crystals embedded with a three-level emitter. These upconversion protocols eliminate the reliance on radiation-pressure coupling, as observed in the downconversion protocol [72], thereby facilitating direct phonon to photon upconversion at the single-phonon level. They operate under an average intracavity photon number substantially below 1, effectively circumventing thermal influences [67–71]. By adjusting the coupling rates, the upconversion efficiency can be precisely controlled, achieving near-optimal efficiency with experimentally achievable parameters [72].

An alternative upconversion protocol can be implemented by driving the auxiliary optical cavity mode with a classical pulse instead of driving the emitter transition, as done in our type-II transducer protocol. In this case, the cavity photon number in the auxiliary mode is larger than 1, and the analytical description based on an effective non-Hermitian Hamiltonian within a subspace is no longer applicable. Instead, numerical simulations using the full master equation can be employed to determine the maximal upconversion efficiency of this protocol [80].

Our type-I quantum transducer uses a single-photon pumping the auxiliary cavity mode, while the type-II quantum transducer is based on a classical pulse pumping the emitter rather than the cavity mode [67,68]. Both protocols prove capable of deterministically transducing single phonons to single photons, for negligible spontaneous decay rates. For practical cavity-enhanced decays compared to spontaneous decays, the upconversion efficiencies of type-I and type-II quantum transducers larger than 90% can be achieved within a bandwidth approximately 0.17Γ and $0.16\Gamma'$ around the resonance frequency, respectively. In principle, the type-II quantum transducer can be generalized to create hybrid entanglement between the phonon and the photon by setting the detuning at a proper value [87], which directly enables distributed hybrid quantum networks by storing the phonon [88] and transmitting the photon to interact with a distant emitter [30–32].

Currently, embedding three-level quantum dots within photonic crystals significantly inhibits coupling to the optical loss mode, enabling α to be minimized [89] and resulting in negligible spontaneous decays of the emitter. In practice, even with a moderated enhanced coupling rate to the

waveguide mode, the variable α remains negligible small [90,91]. Additionally, modern optomechanical crystals are capable of concurrently mitigating losses in both optical and acoustic modes [92,93], facilitating a maximum upconversion efficiency of approximately unity, thereby endorsing the feasibility of high-efficiency single phonon-to-photon quantum transducers.

In summary, we proposed two types of deterministic single phonon-to-photon quantum transducer protocols without radiation-pressure coupling, and showed the feasibility of deterministic phonon-to-photon conversion. This heralds potential applications in the integration of phononic and photonic devices within quantum technologies. Our approach presented an alternative to standard methods used in optomechanical resonators for the development of phonon-to-photon quantum transducers. It thus offers considerable advantages for single phonon detection, making our protocols particularly beneficial for the high-sensitivity detection of single phonons and for large-scale distributed quantum networks.

ACKNOWLEDGMENTS

This work was supported by the National Natural Science Foundation of China (Grants No. 92365107, No. 11904171, and No. 62221004), the National Key R&D Program of China (Grant No. 2019YFA0308700), and the Program for Innovative Talents and Teams in Jiangsu (Grant No. JSSCTD202138).

APPENDIX A: DERIVATION OF THE STATE AMPLITUDES AND THE UPCONVERSION EFFICIENCY OF THE TYPE-I QUANTUM TRANSDUCER

The dynamics of the composite system depicted in Fig. 1 can be described by the Schrödinger equation with the efficient non-Hermitian Hamiltonian $\hat{H}_{\rm eff}$ [81–83]

$$i\hbar\frac{\partial}{\partial t}|\Psi\rangle = \hat{H}_{\rm eff}|\Psi\rangle, \tag{A1}$$

when considering the evolution of the composite system without quantum jumps that collapses the system out of the considered subspace.

For the type-I quantum transducer, by substituting Eqs. (1) and (2) into Eq. (A1), along with the input-output relations [81–83], we can derive the dynamical behavior of the amplitudes C_{21}, C_{32}, C_{31}, and C_3, as shown in Eq. (3). By solving the steady-state solution of Eq. (3), we obtain the following expressions for these amplitudes:

$$C_{21} = \frac{\varepsilon g_{21}\sqrt{2\kappa_{32}} + \sqrt{2}(\sqrt{\kappa_{21}} + \varepsilon\sqrt{\kappa_{32}})S_d}{i\Delta_t S_d + g_{21}^2}\beta_{ka}^{\rm in}, \tag{A2a}$$

$$C_{32} = \frac{i\varepsilon\Delta_t\sqrt{2\kappa_{32}} - \sqrt{2}g_{21}(\sqrt{\kappa_{21}} + \varepsilon\sqrt{\kappa_{32}})}{i\varepsilon\Delta_t S_d + \varepsilon g_{21}^2}\beta_{kb}^{\rm in}, \tag{A2b}$$

$$C_{31} = \frac{\sqrt{2}g_{31}g_{32}[g_{21}(\sqrt{\kappa_{21}} + \varepsilon\sqrt{\kappa_{32}}) - i\varepsilon\sqrt{\kappa_{32}}\Delta_t]}{G\left(i\Delta_t S_d + g_{21}^2\right)}\beta_{ka}^{\rm in}. \tag{A2c}$$

Now, combining with Eq. (4), we obtain the output amplitudes

$$\begin{aligned}\beta_{ka}^{\rm out} &= \sqrt{2\kappa_{21}}C_{21} - \beta_{ka}^{\rm in}\\ &= \left\{\frac{2[\varepsilon g_{21}\sqrt{\kappa_{21}\kappa_{32}} + (\varepsilon\sqrt{\kappa_{21}\kappa_{32}} + \kappa_{21})S_d]}{i\Delta_t S_d + g_{21}^2} - 1\right\}\beta_{ka}^{\rm in}\\ &= t_{21}\beta_{ka}^{\rm in},\end{aligned} \tag{A3}$$

$$\begin{aligned}\beta_{kb}^{\rm out} &= \sqrt{2\kappa_{32}}C_{32} - \beta_{kb}^{\rm in}\\ &= \left\{\frac{2[i\varepsilon\kappa_{32}\Delta_t - g_{21}(\sqrt{\kappa_{21}\kappa_{32}} + \varepsilon\kappa_{32})]}{\varepsilon\left(i\Delta_t S_d + g_{21}^2\right)} - 1\right\}\beta_{kb}^{\rm in}\\ &= t_{32}\beta_{kb}^{\rm in},\end{aligned} \tag{A4}$$

$$\begin{aligned}\beta_{ka}^{\rm out'} &= \sqrt{2\kappa_{31}}C_{31}\\ &= \frac{2g_{31}g_{32}\sqrt{\kappa_{31}}[g_{21}(\sqrt{\kappa_{21}} + \varepsilon\sqrt{\kappa_{32}}) - i\varepsilon\sqrt{\kappa_{32}}\Delta_t]}{G\left(i\Delta_t S_d + g_{21}^2\right)}\beta_{ka}^{\rm in}\\ &= t_{31}\beta_{ka}^{\rm in}.\end{aligned} \tag{A5}$$

We can thus directly obtain the transmission coefficients t_{21}, t_{32}, and t_{31}, as shown in Eqs. (5) to (7).

To achieve the maximal quantum upconversion efficiency for vanishing detunings (i.e., $\delta_{21} = \delta_{31} = \Delta_{\rm a} = \Delta_{\rm b} = \Delta_{\rm c} = 0$) and $\varepsilon = -1$, we have $\Delta_t' = -i(\kappa_{21} + \kappa_{32})$, $G' = g_{31}^2 + \kappa_{31}\gamma_3/2$, $S_d' = g_{32}^2/(g_{31}^2/\kappa_{31} + \gamma_3/2) + \kappa_{32} + \gamma_2/2$. We assume $t_{21} = 0$ and $t_{32} = 0$, which results in the following two relationships:

$$\zeta = -2[g_{21}\sqrt{\kappa_{21}\kappa_{32}} + (\sqrt{\kappa_{21}\kappa_{32}} - \kappa_{21})S_d'], \tag{A6}$$

$$\zeta = 2[g_{21}(\sqrt{\kappa_{21}\kappa_{32}} - \kappa_{32}) + i\kappa_{32}\Delta_t'], \tag{A7}$$

where we introduce the auxiliary parameter $\zeta = i\Delta_t' S_d' + g_{21}^2$ for simplicity.

After a straightforward transformation of Eq. (A7), we arrive at the boundary condition for the cavity-enhanced spontaneous decays that allows for the maximization of the upconversion efficiency as follows:

$$\begin{aligned}1 - \frac{\Gamma_{32}}{\gamma_3 + \Gamma_{31}} &= \frac{2g_{21}\left(1 - \sqrt{\frac{\kappa_{21}}{\kappa_{32}}}\right)}{\kappa_{21} + \kappa_{32}} + \frac{2g_{21}^2 + \gamma_2(\kappa_{21} + \kappa_{32})}{2\kappa_{32}(\kappa_{21} + \kappa_{32})}\\ &> 0,\end{aligned} \tag{A8}$$

where $\Gamma_{32} < \gamma_3 + \Gamma_{31}$ holds for practical parameters (i.e., $\kappa_{32} \gg \kappa_{21}, g_{21} > 0$) used in our protocol.

The upconversion efficiency $\eta_{si} = |t_{31}|^2$ for our type-I quantum transducer can be significantly simplified by incorporating Eqs. (A6) and (A7), and then specified as

$$\begin{aligned}\eta_{si} &= \left|\frac{2g_{31}g_{32}\sqrt{\kappa_{31}}[g_{21}(\sqrt{\kappa_{21}} - \sqrt{\kappa_{32}}) + i\sqrt{\kappa_{32}}\Delta_t']}{G'\zeta}\right|^2\\ &= \frac{4\kappa_{31}(g_{31}g_{32})^2}{\kappa_{32}\left(2g_{31}^2 + \kappa_{31}\gamma_3\right)^2}\\ &= \frac{\Gamma_{31}\Gamma_{32}}{(\gamma_3 + \Gamma_{31})^2},\end{aligned} \tag{A9}$$

where we use cavity-enhanced decay rates $\Gamma_{32} = 2g_{32}^2/\kappa_{32}$ and $\Gamma_{31} = 2g_{31}^2/\kappa_{31}$ for simplicity. Therefore, for practical parameters, the upconversion efficiency η_{si} of our type-I quantum transducer can only approach unity from the lower side.

APPENDIX B: DERIVATION OF THE STATE AMPLITUDES AND THE UPCONVERSION EFFICIENCY OF THE TYPE-II QUANTUM TRANSDUCER

For the type-II quantum transducer, the equations of motion for the state amplitudes, as shown in Eq. (11), can be obtained in a similar way by incorporating the input-output relations into the Schrödinger equation [81–83]. By solving the steady-state solution, we can obtain the state amplitudes as follows:

$$C_{21} = \frac{i\sqrt{2\kappa_{21}}(4\tilde{\delta}_{21}G + \Omega^2\tilde{\Delta}_c)}{4g_{21}^2 G - \tilde{\Delta}_a(4\tilde{\delta}_{21}G + \Omega^2\tilde{\Delta}_c)}\beta_k^{\text{in}}, \tag{B1}$$

$$C_{31} = -\frac{2i\Omega g_{21}g_{31}\sqrt{2\kappa_{21}}}{4g_{21}^2 G - \tilde{\Delta}_a(4\tilde{\delta}_{21}G + \Omega^2\tilde{\Delta}_c)}\beta_k^{\text{in}}. \tag{B2}$$

By combining with Eq. (12), the output amplitudes can be specified as follows:

$$\begin{aligned}\beta_k^{\text{out}} &= \sqrt{2\kappa_{21}}C_{21} - \beta_k^{\text{in}} \\ &= \left[\frac{2i\kappa_{21}(4\tilde{\delta}_{21}G + \Omega^2\tilde{\Delta}_c)}{4g_{21}^2 G - \tilde{\Delta}_a(4\tilde{\delta}_{21}G + \Omega^2\tilde{\Delta}_c)} - 1\right]\beta_k^{\text{in}} \\ &= t'_{21}\beta_k^{\text{in}},\end{aligned} \tag{B3}$$

$$\begin{aligned}\beta_k^{\text{out}'} &= \sqrt{2\kappa_{31}}C_{31} \\ &= -\frac{4i\Omega g_{21}g_{31}\sqrt{\kappa_{21}\kappa_{31}}}{4g_{21}^2 G - \tilde{\Delta}_a(4\tilde{\delta}_{21}G + \Omega^2\tilde{\Delta}_c)}\beta_k^{\text{in}} \\ &= t'_{31}\beta_k^{\text{in}}.\end{aligned} \tag{B4}$$

Therefore, we can directly obtain the transmission coefficients t'_{21} and t'_{31}, as shown in Eqs. (13) and (14).

To achieve the maximal quantum upconversion efficiency for vanishing detunings (i.e., $\delta_{21} = \delta_{31} = \Delta_a = \Delta_b = \Delta_c = 0$), we have the following relationships: $\Delta'_t = -i(\kappa_{21} + \kappa_{32})$, $G' = g_{31}^2 + \kappa_{31}\gamma_3/2$, $S'_d = g_{32}^2/(g_{31}^2/\kappa_{31} + \gamma_3/2) + \kappa_{32} + \gamma_2/2$. The transmission coefficient for the phonon is $t_{21} = 0$, leading directly to the following equation:

$$0 = 4g_{21}^2 G' - (\tilde{\Delta}'_a + 2i\kappa_{21})(4\tilde{\delta}'_{21}G' + \Omega^2\tilde{\Delta}'_c). \tag{B5}$$

After a straightforward transformation of Eq. (B5), we have

$$\left(\frac{\Gamma_{21}}{2} - \frac{\gamma_2}{2}\right)\left(\frac{\gamma_3}{2} + \frac{\Gamma_{31}}{2}\right) - \frac{\Omega^2}{4} = 0, \tag{B6}$$

where we use the parameters $\Gamma_{21} = 2g_{21}^2/\kappa_{21}$ and $\Gamma_{31} = 2g_{31}^2/\kappa_{31}$ for simplicity.

The condition for the Rabi frequency Ω of the laser pulse that allows for the maximization of the upconversion efficiency can thus be specified as follows:

$$\Omega = \sqrt{(\Gamma_{21} - \gamma_2)(\Gamma_{31} + \gamma_3)}. \tag{B7}$$

The upconversion efficiency η_{ci} for the type-II quantum transducer can thus be simplified by incorporating the above condition for the Rabi frequency Ω as follows:

$$\begin{aligned}\eta_{ci} = |t'_{31}|^2 &= \left|-\frac{4i\Omega g_{21}g_{31}\sqrt{\kappa_{21}\kappa_{31}}}{4g_{21}^2 G' - \tilde{\Delta}'_a(4\tilde{\delta}'_{21}G' + \Omega^2\tilde{\Delta}'_c)}\right|^2 \\ &= \frac{(\Gamma_{21} - \gamma_2)\Gamma_{31}}{\Gamma_{21}(\Gamma_{31} + \gamma_3)} \\ &= \frac{1 - \frac{\gamma_2}{\Gamma_{21}}}{1 + \frac{\gamma_3}{\Gamma_{31}}},\end{aligned} \tag{B8}$$

which also can approaches unity for negligible spontaneous decays, leading to a deterministic upconversion quantum transducer.

[1] Z.-L. Xiang, S. Ashhab, J. Q. You, and F. Nori, Hybrid quantum circuits: Superconducting circuits interacting with other quantum systems, Rev. Mod. Phys. **85**, 623 (2013).

[2] I. Buluta, S. Ashhab, and F. Nori, Natural and artificial atoms for quantum computation, Rep. Prog. Phys. **74**, 104401 (2011).

[3] P.-B. Li, Z.-L. Xiang, P. Rabl, and F. Nori, Hybrid quantum device with nitrogen-vacancy centers in diamond coupled to carbon nanotubes, Phys. Rev. Lett. **117**, 015502 (2016).

[4] H.-R. Wei and F.-G. Deng, Universal quantum gates for hybrid systems assisted by quantum dots inside double-sided optical microcavities, Phys. Rev. A **87**, 022305 (2013).

[5] J. Twamley and S. D. Barrett, Superconducting cavity bus for single nitrogen-vacancy defect centers in diamond, Phys. Rev. B **81**, 241202(R) (2010).

[6] B. Sarma, T. Busch, and J. Twamley, Cavity magnomechanical storage and retrieval of quantum states, New J. Phys. **23**, 043041 (2021).

[7] Y.-W. Lu, J.-F. Liu, Z. Liao, and X.-H. Wang, Plasmonic-photonic cavity for high-efficiency single-photon blockade, Sci. China Phys. Mech. Astron. **64**, 274212 (2021).

[8] J. Li, Z. Xie, Y. Li, Y. Liang, Z. Li, and T. Li, Heralded entanglement between error-protected logical qubits for fault-tolerant distributed quantum computing, Sci. China Phys. Mech. Astron. **67**, 220311 (2024).

[9] P. Zhao, W. Zhong, M.-M. Du, X.-Y. Li, L. Zhou, and Y.-B. Sheng, Quantum secure direct communication with hybrid entanglement, Front. Phys. **19**, 51201 (2024).

[10] W. Qin, A. F. Kockum, C. S. Muñoz, A. Miranowicz, and F. Nori, Quantum amplification and simulation of strong and ultrastrong coupling of light and matter, Phys. Rep. **1078**, 1 (2024).

[11] J.-Q. You and F. Nori, Atomic physics and quantum optics using superconducting circuits, Nature (London) **474**, 589 (2011).

[12] A. F. Kockum and F. Nori, Quantum bits with Josephson junctions, in *Fundamentals and Frontiers of the Josephson Effect*, edited by F. Tafuri (Springer, New York, 2019), pp. 703–741.

[13] F. Arute *et al.*, Quantum supremacy using a programmable superconducting processor, Nature (London) **574**, 505 (2019).

[14] Y. Ma, Y. Xu, X. Mu, W. Cai, L. Hu, W. Wang, X. Pan, H. Wang, Y. P. Song, C. L. Zou, and L. Sun, Error-transparent

operations on a logical qubit protected by quantum error correction, Nat. Phys. **16**, 827 (2020).
[15] Y. Zhao *et al.*, Realization of an error-correcting surface code with superconducting qubits, Phys. Rev. Lett. **129**, 030501 (2022).
[16] Google Quantum AI, Suppressing quantum errors by scaling a surface code logical qubit, Nature (London) **614**, 676 (2023).
[17] Z. Ni *et al.*, Beating the break-even point with a discrete-variable-encoded logical qubit, Nature (London) **616**, 56 (2023).
[18] Z.-L. Xiang, M. Zhang, L. Jiang, and P. Rabl, Intracity quantum communication via thermal microwave networks, Phys. Rev. X **7**, 011035 (2017).
[19] Z. Guo, Z. Xie, Y. Wang, Z. Li, and T. Li, Heralded and robust W-state generation for distant superconducting qubits with practical microwave pulse scattering, Appl. Phys. Lett. **123**, 264002 (2023).
[20] Y. Zhong *et al.*, Deterministic multi-qubit entanglement in a quantum network, Nature (London) **590**, 571 (2021).
[21] S. Storz *et al.*, Loophole-free Bell inequality violation with superconducting circuits, Nature (London) **617**, 265 (2023).
[22] D. Awschalom *et al.*, Development of quantum interconnects (QuICs) for next-generation information technologies, PRX Quantum **2**, 017002 (2021).
[23] W. Zhang, D.-S. Ding, Y.-B. Sheng, L. Zhou, B.-S. Shi, and G.-C. Guo, Quantum secure direct communication with quantum memory, Phys. Rev. Lett. **118**, 220501 (2017).
[24] J. Yuan, X. Wang, G. Chen, L. Wang, L. Xiao, and S. Jia, High-fidelity frequency converter in high-dimensional spaces, Laser Photon. Rev. **18**, 2400368 (2024).
[25] Y.-G. Liu, K. Xia, and S.-L. Zhu, Efficient microwave-to-optical single-photon conversion with a single flying circular Rydberg atom, Opt. Express **29**, 9942 (2021).
[26] W. Z. Jia, Y. W. Wang, and Y.-X. Liu, Efficient single-photon frequency conversion in the microwave domain using superconducting quantum circuits, Phys. Rev. A **96**, 053832 (2017).
[27] J. Holzgrafe, N. Sinclair, D. Zhu, A. Shams-Ansari, M. Colangelo, Y. Hu, M. Zhang, K. K. Berggren, and M. Lončar, Cavity electro-optics in thin-film lithium niobate for efficient microwave-to-optical transduction, Optica **7**, 1714 (2020).
[28] X. Han, W. Fu, C.-L. Zou, L. Jiang, and H. X. Tang, Microwave-optical quantum frequency conversion, Optica **8**, 1050 (2021).
[29] J. I. Cirac, A. K. Ekert, S. F. Huelga, and C. Macchiavello, Distributed quantum computation over noisy channels, Phys. Rev. A **59**, 4249 (1999).
[30] N. Lo Piparo, M. Hanks, C. Gravel, K. Nemoto, and W. J. Munro, Resource reduction for distributed quantum information processing using quantum multiplexed photons, Phys. Rev. Lett. **124**, 210503 (2020).
[31] H. Zhou, T. Li, and K. Xia, Parallel and heralded multiqubit entanglement generation for quantum networks, Phys. Rev. A **107**, 022428 (2023).
[32] S. Wehner, D. Elkouss, and R. Hanson, Quantum internet: A vision for the road ahead, Science **362**, eaam9288 (2018).
[33] M. Aspelmeyer, T. J. Kippenberg, and F. Marquardt, Cavity optomechanics, Rev. Mod. Phys. **86**, 1391 (2014).
[34] H. Jing, S. K. Özdemir, X.-Y. Lü, J. Zhang, L. Yang, and F. Nori, $\mathcal{PT}$-symmetric phonon laser, Phys. Rev. Lett. **113**, 053604 (2014).
[35] X.-Y. Lü, H. Jing, J.-Y. Ma, and Y. Wu, $\mathcal{PT}$-symmetry-breaking chaos in optomechanics, Phys. Rev. Lett. **114**, 253601 (2015).
[36] Z. Shen, Y.-L. Zhang, Y. Chen, C.-L. Zou, Y.-F. Xiao, X.-B. Zou, F.-W. Sun, G.-C. Guo, and C.-H. Dong, Experimental realization of optomechanically induced non-reciprocity, Nat. Photon. **10**, 657 (2016).
[37] L.-L. Zheng, T.-S. Yin, Q. Bin, X.-Y. Lü, and Y. Wu, Single-photon-induced phonon blockade in a hybrid spin-optomechanical system, Phys. Rev. A **99**, 013804 (2019).
[38] Y. Wang, J.-L. Wu, J.-X. Han, Y. Xia, Y.-Y. Jiang, and J. Song, Enhanced phonon blockade in a weakly coupled hybrid system via mechanical parametric amplification, Phys. Rev. Appl. **17**, 024009 (2022).
[39] Z. Shen, Y.-L. Zhang, Y. Chen, F.-W. Sun, X.-B. Zou, G.-C. Guo, C.-L. Zou, and C.-H. Dong, Reconfigurable optomechanical circulator and directional amplifier, Nat. Commun. **9**, 1797 (2018).
[40] J. Tang, Y. Wu, Z. Wang, H. Sun, L. Tang, H. Zhang, T. Li, Y. Lu, M. Xiao, and K. Xia, Vacuum-induced surface-acoustic-wave phonon blockade, Phys. Rev. A **101**, 053802 (2020).
[41] D. Y. Wang, C. H. Bai, Y. Xing, S. Liu, S. Zhang, and H. F. Wang, Enhanced photon blockade via driving a trapped Λ-type atom in a hybrid optomechanical system, Phys. Rev. A **102**, 043705 (2020).
[42] Y.-P. Gao and C. Wang, Hybrid coupling optomechanical assisted nonreciprocal photon blockade, Opt. Express **29**, 25161 (2021).
[43] K. Wang, Y.-P. Gao, R. Jiao, and C. Wang, Recent progress on optomagnetic coupling and optical manipulation based on cavity-optomagnonics, Front. Phys. **17**, 42201 (2022).
[44] L. A. Kanari-Naish, J. Clarke, S. Qvarfort, and M. R. Vanner, Two-mode Schrödinger-cat states with nonlinear optomechanics: generation and verification of non-Gaussian mechanical entanglement, Quantum Sci. Technol. **7**, 035012 (2022).
[45] J. Clarke, P. Neveu, K. E. Khosla, E. Verhagen, and M. R. Vanner, Cavity quantum optomechanical nonlinearities and position measurement beyond the breakdown of the linearized approximation, Phys. Rev. Lett. **131**, 053601 (2023).
[46] M. C. Kuzyk and H. Wang, Scaling phononic quantum networks of solid-state spins with closed mechanical subsystems, Phys. Rev. X **8**, 041027 (2018).
[47] Z.-Q. Yin, W. L. Yang, L. Sun, and L. M. Duan, Quantum network of superconducting qubits through an optomechanical interface, Phys. Rev. A **91**, 012333 (2015).
[48] M.-A. Lemonde, S. Meesala, A. Sipahigil, M. J. A. Schuetz, M. D. Lukin, M. Loncar, and P. Rabl, Phonon networks with silicon-vacancy centers in diamond waveguides, Phys. Rev. Lett. **120**, 213603 (2018).
[49] J. Li, Y.-P. Wang, W.-J. Wu, S.-Y. Zhu, and J. Q. You, Quantum network with magnonic and mechanical nodes, PRX Quantum **2**, 040344 (2021).
[50] H. Qiao *et al.*, Splitting phonons: Building a platform for linear mechanical quantum computing, Science **380**, 1030 (2023).
[51] I. Arrazola, Y. Minoguchi, M.-A. Lemonde, A. Sipahigil, and P. Rabl, Toward high-fidelity quantum information processing and quantum simulation with spin qubits and phonons, Phys. Rev. B **110**, 045419 (2024).
[52] H. Flayac and V. Savona, Heralded preparation and readout of entangled phonons in a photonic crystal cavity, Phys. Rev. Lett. **113**, 143603 (2014).

[53] X.-Y. Lü, G.-L. Zhu, L.-L. Zheng, and Y. Wu, Entanglement and quantum superposition induced by a single photon, Phys. Rev. A **97**, 033807 (2018).

[54] F. Zou, J.-Q. Liao, and Y. Li, Dynamical emission of phonon pairs in optomechanical systems, Phys. Rev. A **105**, 053507 (2022).

[55] D.-G. Lai, J.-Q. Liao, A. Miranowicz, and F. Nori, Noise-tolerant optomechanical entanglement via synthetic magnetism, Phys. Rev. Lett. **129**, 063602 (2022).

[56] J. Huang, D.-G. Lai, and J.-Q. Liao, Controllable generation of mechanical quadrature squeezing via dark-mode engineering in cavity optomechanics, Phys. Rev. A **108**, 013516 (2023).

[57] T.-T. Ma, Y.-Q. Liu, and C.-S. Yu, Release of virtual photon and phonon pairs from qubit-plasmon-phonon ultrastrong coupling system, Opt. Express **31**, 30832 (2023).

[58] Y.-X. Ma and P.-B. Li, Deterministic generation of phononic fock states via weak nonlinearities, Phys. Rev. A **108**, 053709 (2023).

[59] P. Rabl, P. Cappellaro, M. V. Gurudev Dutt, L. Jiang, J. R. Maze, and M. D. Lukin, Strong magnetic coupling between an electronic spin qubit and a mechanical resonator, Phys. Rev. B **79**, 041302(R) (2009).

[60] S. D. Bennett, N. Y. Yao, J. Otterbach, P. Zoller, P. Rabl, and M. D. Lukin, Phonon-induced spin-spin interactions in diamond nanostructures: Application to spin squeezing, Phys. Rev. Lett. **110**, 156402 (2013).

[61] P.-B. Li, Y. Zhou, W.-B. Gao, and F. Nori, Enhancing spin-phonon and spin-spin interactions using linear resources in a hybrid quantum system, Phys. Rev. Lett. **125**, 153602 (2020).

[62] M. Abdi and M. B. Plenio, Quantum effects in a mechanically modulated single-photon emitter, Phys. Rev. Lett. **122**, 023602 (2019).

[63] Y.-P. Gao, C. Cao, T.-J. Wang, Y. Zhang, and C. Wang, Cavity-mediated coupling of phonons and magnons, Phys. Rev. A **96**, 023826 (2017).

[64] J. Li, S.-Y. Zhu, and G. S. Agarwal, Magnon-photon-phonon entanglement in cavity magnomechanics, Phys. Rev. Lett. **121**, 203601 (2018).

[65] W. Xie, Q. Guo, and Z. Duan, Phonon blockade in an acoustic cavity coupled to a three-level artificial atom, Phys. Rev. B **106**, 115435 (2022).

[66] X.-L. Hei, P.-B. Li, X.-F. Pan, and F. Nori, Enhanced tripartite interactions in spin-magnon-mechanical hybrid systems, Phys. Rev. Lett. **130**, 073602 (2023).

[67] M. Mirhosseini, A. Sipahigil, M. Kalaee, and O. Painter, Superconducting qubit to optical photon transduction, Nature (London) **588**, 599 (2020).

[68] C. Galland, N. Sangouard, N. Piro, N. Gisin, and T. J. Kippenberg, Heralded single-phonon preparation, storage, and readout in cavity optomechanics, Phys. Rev. Lett. **112**, 143602 (2014).

[69] S. M. Meenehan, J. D. Cohen, G. S. MacCabe, F. Marsili, M. D. Shaw, and O. Painter, Pulsed excitation dynamics of an optomechanical crystal resonator near its quantum ground state of motion, Phys. Rev. X **5**, 041002 (2015).

[70] S. Hong, R. Riedinger, I. Marinković, A. Wallucks, S. G. Hofer, R. A. Norte, M. Aspelmeyer, and S. Gröblacher, Hanbury Brown and Twiss interferometry of single phonons from an optomechanical resonator, Science **358**, 203 (2017).

[71] A. H. Safavi-Naeini and O. Painter, Proposal for an optomechanical traveling wave phonon–photon translator, New J. Phys. **13**, 013017 (2011).

[72] I. Söllner, L. Midolo, and P. Lodahl, Deterministic single-phonon source triggered by a single photon, Phys. Rev. Lett. **116**, 234301 (2016).

[73] S. M. Meenehan, J. D. Cohen, S. Gröblacher, J. T. Hill, A. H. Safavi-Naeini, M. Aspelmeyer, and O. Painter, Silicon optomechanical crystal resonator at millikelvin temperatures, Phys. Rev. A **90**, 011803(R) (2014).

[74] S. Mohammadi, A. A. Eftekhar, A. Khelif, and A. Adibi, Simultaneous two-dimensional phononic and photonic band gaps in opto-mechanical crystal slabs, Opt. Express **18**, 9164 (2010).

[75] J. Dalibard, Y. Castin, and K. Mølmer, Wave-function approach to dissipative processes in quantum optics, Phys. Rev. Lett. **68**, 580 (1992).

[76] K. Xia and J. Twamley, All-optical switching and router via the direct quantum control of coupling between cavity modes, Phys. Rev. X **3**, 031013 (2013).

[77] K. Xia, G. Lu, G. Lin, Y. Cheng, Y. Niu, S. Gong, and J. Twamley, Reversible nonmagnetic single-photon isolation using unbalanced quantum coupling, Phys. Rev. A **90**, 043802 (2014).

[78] D. Witthaut and A. S. Sørensen, Photon scattering by a three-level emitter in a one-dimensional waveguide, New J. Phys. **12**, 043052 (2010).

[79] L. Tang, J. Tang, W. Zhang, G. Lu, H. Zhang, Y. Zhang, K. Xia, and M. Xiao, On-chip chiral single-photon interface: Isolation and unidirectional emission, Phys. Rev. A **99**, 043833 (2019).

[80] D. Roy, C. M. Wilson, and O. Firstenberg, Colloquium: Strongly interacting photons in one-dimensional continuum, Rev. Mod. Phys. **89**, 021001 (2017).

[81] S. Das, A. Grankin, I. Iakoupov, E. Brion, J. Borregaard, R. Boddeda, I. Usmani, A. Ourjoumtsev, P. Grangier, and A. S. Sørensen, Photonic controlled-phase gates through Rydberg blockade in optical cavities, Phys. Rev. A **93**, 040303(R) (2016).

[82] T. Li and G.-L. Long, Hyperparallel optical quantum computation assisted by atomic ensembles embedded in double-sided optical cavities, Phys. Rev. A **94**, 022343 (2016).

[83] I. Cohen and K. Mølmer, Deterministic quantum network for distributed entanglement and quantum computation, Phys. Rev. A **98**, 030302(R) (2018).

[84] S. Fan, Ş. E. Kocabaş, and J.-T. Shen, Input-output formalism for few-photon transport in one-dimensional nanophotonic waveguides coupled to a qubit, Phys. Rev. A **82**, 063821 (2010).

[85] E. Rephaeli and S. Fan, Dissipation in few-photon waveguide transport [invited], Photon. Res. **1**, 110 (2013).

[86] C. Spinnler, G. N. Nguyen, Y. Wang, L. Zhai, A. Javadi, M. Erbe, S. Scholz, A. D. Wieck, A. Ludwig, P. Lodahl, L. Midolo, and R. J. Warburton, A single-photon emitter coupled to a phononic-crystal resonator in the resolved-sideband regime, Nat. Commun. **15**, 9509 (2024).

[87] T. Li, A. Miranowicz, X. Hu, K. Xia, and F. Nori, Quantum memory and gates using a Λ-type quantum emitter coupled to a chiral waveguide, Phys. Rev. A **97**, 062318 (2018).

[88] G. S. MacCabe, H. Ren, J. Luo, J. D. Cohen, H. Zhou, A. Sipahigil, M. Mirhosseini, and O. Painter, Nano-acoustic resonator with ultralong phonon lifetime, Science **370**, 840 (2020).

[89] P. Lodahl, S. Mahmoodian, and S. Stobbe, Interfacing single photons and single quantum dots with photonic nanostructures, Rev. Mod. Phys. **87**, 347 (2015).

[90] Q. Wang, S. Stobbe, and P. Lodahl, Mapping the local density of optical states of a photonic crystal with single quantum dots, Phys. Rev. Lett. **107**, 167404 (2011).

[91] M. Arcari, I. Söllner, A. Javadi, S. Lindskov Hansen, S. Mahmoodian, J. Liu, H. Thyrrestrup, E. H. Lee, J. D. Song, S. Stobbe, and P. Lodahl, Near-unity coupling efficiency of a quantum emitter to a photonic crystal waveguide, Phys. Rev. Lett. **113**, 093603 (2014).

[92] A. H. Safavi-Naeini and O. Painter, Design of optomechanical cavities and waveguides on a simultaneous bandgap phononic-photonic crystal slab, Opt. Express **18**, 14926 (2010).

[93] X. Ma, P. K. Shandilya, and P. E. Barclay, Semiconductor-on-diamond cavities for spin optomechanics, Opt. Express **31**, 22470 (2023).